Available online at www.sciencedirect.com
ScienceDirect
Journal of Sound and Vibration 306 (2007) 507–523
JOURNAL OF SOUND AND VIBRATION
www.elsevier.com/locate/jsvi

On the propagation of acoustic energy in the vicinity of a bubble chain

Aneta Nikolovska[a], Richard Manasseh[b,*], Andrew Ooi[a]

[a]*Department of Mechanical & Manufacturing Engineering, University of Melbourne, VIC 3010, Melbourne, Australia*
[b]*Fluid Dynamics Group, CSIRO, P.O. Box 56, Highett, VIC 3190, Melbourne, Australia*[1]

Received 17 January 2006; received in revised form 6 February 2007; accepted 13 May 2007
Available online 13 August 2007

Abstract

In this paper, experimental data on the propagation of acoustic energy in the vicinity of a vertical chain of discrete air bubbles are presented. The acoustic energy was created naturally during the formation of each bubble at the bottom of the chain. Previous work has reported that the root-mean-squared pressure distribution is highly anisotropic in the vicinity of a bubble chain. A new experimental set-up has been developed to obtain 'snapshots' of the instantaneous acoustic pressure field using a triggering technique with two hydrophones. This methodology allowed coordinated measurement of the acoustic signal in the near and far field and the data were used to construct the instantaneous spatial distribution of acoustic energy around the bubble chains. The results show that the phase speed in the direction of the bubble chain has values substantially lower than the speed of sound in pure water. Bubble chains of different configurations were investigated and it was found that this speed of propagation is reduced for chains consisting of larger and more closely spaced bubbles.

1. Introduction

Acoustic energy is capable of being transmitted through the sea to distances that are significant to oceanographic and marine exploration [1–3]. Because of this, sound is used for underwater communications, antisubmarine warfare, and underwater navigation. The large difference in characteristic impedance between the air and the water make bubbles very efficient as reflectors of acoustic energy in water. Very little sound will penetrate a curtain of air bubbles, making them very effective as camouflage for noise sources. A single bubble has little impact on the transmission of sound, but an assembly of bubbles introduces significant changes to the acoustic properties of the host medium [4,5]. When sound traverses a cluster of bubbles, every bubble produces a secondary scattered wave and these waves reinforce in some directions and interfere in others [6,7]; this gives rise to coherent, incoherent, and multiple scattering.

*Corresponding author. Fax: +61 3 9252 6586.
E-mail address: Richard.Manasseh@csiro.au (R. Manasseh).
[1]CSIRO: Commonwealth Scientific and Industrial Research Organisation.

0022-460X/$ - see front matter
doi:10.1016/j.jsv.2007.05.025

The size and distribution of bubbles in the medium has a strong influence on physical properties of the system, such as the rate of gas–liquid mass transfer [8–10] or the energy dissipation of ocean breakers [11]. In active bubble acoustics, sound is sent into the system and the propagation of the resulting signals is interpreted to infer the bubble-size distribution or other properties of the system. The 'continuum' (averaged) acoustic properties of bubbly flows [12] have been the basis of several instruments for oceanographic and industrial applications [13–17] although none are in widespread use. An obvious limitation of these theories is the assumption that the bubbles are uniformly distributed. In reality, the distribution of bubbles in a liquid is rarely isotropic or homogeneous and thus the propagation of sound is rarely isotropic. Even in passive or 'listening' systems, sound could be more efficiently channelled along chains of bubbles [18], impairing interpretation of the data when there is a non-isotropic distribution of bubbles. Hence, a better understanding of the variation of sound speed in a complex bubbly flow could lead to better instruments for industrial and oceanographic applications. For completeness, it must be mentioned here that the bubble chain also exhibits many interesting hydrodynamic properties and the hydrodynamic stability of bubble chains has been investigated by Ruzicka [19].

The choice of the appropriate theoretical model for the acoustic field of a bubble chain system is a topic that has been investigated by many researchers, focussing primarily on coupled-oscillator approximations. Important works include those of Zabolotskaya [20], Ogũz and Prosperetti [21], Doinikov and Zavtrak [22], Tolstoy [23,24], Feuillade [6,25] and Ida [26]. From a theoretical point of view there have been a number of earlier works on the behaviour of different configurations of bubble systems [27,28]. In 1966, Weston [29] first considered the frequency response of a line of air bubbles. He derived approximate formulas for sound scattered by an air-bubble as a cell of an array and predicted that the line array of bubbles displays properties like a cylindrical bubble; this work was continued by Tolstoy [23]. Later, bubbles embedded in a line array were also numerically studied by Feuillade [30] and Tolstoy [24]. The emergence of super- and quasi-resonances was a new phenomenon associated with the line and plane structures [23,25] predicting that enhanced resonances can be observed in these bubble systems. The models have been validated for the two and three bubble case by comparing the predicted natural frequencies with experimental data [31,32].

Few cases of more than two bubbles (distributed in an anisotropic fashion) have been studied. Manasseh et al. [18] reported an anisotropic sound field around a bubble chain by simply comparing rms pressures along horizontal and vertical lines, and suggested that a coupled-oscillator model could qualitatively explain the anisotropy. Doinikov et al. [33] subsequently improved the comparison with experiment by introducing time delays to the model.

It is well known that the speed of sound in a bubbly medium can be dramatically reduced from the speed in pure water [34], based simply on the averaged compressibility and density of an air–water mixture. Much work (e.g. Ref. [12]) has been done to predict sound speeds in homogenous bubbly media where bubble resonances are also taken into account. Even though there has been many theoretical models predicting the frequency response of discrete bubbly systems, the authors are unaware of any experimental studies on the channelling of acoustic energy and the propagation speed of this energy near discrete anisotropic bubbly structures. In the system investigated here, the bubbles are arranged in an almost vertical line and they originate from a nozzle at the bottom of the bubble chain. Acoustic energy is generated when a bubble detaches at the nozzle and this energy is guided along the chain of discrete bubbles. The energy is in the form of a discrete pulse of sound that typically dies off in 10–20 ms, and depending on the bubble production rate (BPR), these pulses are typically separated by 30–100 ms, so that the pulses never overlap. This paper provides high-resolution experimental data showing instantaneous snapshots of the spatial distribution of the acoustic energy around the bubble chain. The data were obtained by a new experimental system using a coordinated robotic traverse and acoustically triggered data acquisition system.

In summary, the phenomenon of anisotropic sound propagation along a bubble chain is a special case of a more general situation in which sound propagates through a medium in which bubbles are distributed inhomogeneously. It is possible to model the acoustics of arrays of finite numbers of bubbles by reducing the equations of motion to a set of coupled oscillators [6,20,25,26]. Furthermore, Manasseh et al. [18] and Doinikov et al. [33] showed that a bubble chain transmits sound anisotropically because the coupled oscillators effectively behave like a set of masses hanging on springs. If the oscillators are arranged in a line and all connected together, a point vibration initiated at one end travels to the other end without the reduction

in amplitude that spherical propagation from a point source normally entails. Each bubble re-radiates sound as the disturbance passes and the result is an anisotropic sound field with the sound very efficiently 'channelled' along the chain. In the present experiments, as in Refs. [17,18,33,36,37], the exciting signal is provided naturally by the formation sound of each bubble at the base of the chain.

The first part of this paper will describe in detail the characteristics of the measurement system designed for this purpose. The second part will concentrate on the acoustic variables measured for several different bubble chain configurations generated by two different sized nozzles and at different airflow rates. Finally, data on the propagation of acoustic energy and sound attenuation along the bubble chain will be summarized.

2. Experimental approach

2.1. Bubble production and hydrophone scanning method

A system for producing discretely distributed air bubbles in water was designed and constructed. The complete experimental set-up is shown in Fig. 1. Air bubbles were produced with a system similar to that described in Manasseh [17]. The nozzles used for bubble production, which have a 2.500 ± 0.025 and 1.000 ± 0.025 mm internal orifice diameter, was supplied with air via a precision pressure regulator (CompAir Maxam type A216) at 13 ± 5 kPa pressure. To ensure a known contact radius during bubble formation, the edge of the nozzles were machined to be as sharp as possible.

A hydrophone-scanning procedure based on a fixed hydrophone near the nozzle and a moveable hydrophone was used to simultaneously acquire the sound pulse generated on bubble formation from both the near and far field. The fixed hydrophone effectively acted as a trigger, monitoring the exciting signal from the newly formed bubble at the nozzle and starting acquisition simultaneously from both hydrophones. Bruel & Kjaer type 8103 hydrophones were used for data acquisition. They have a linear response in the 1 kHz frequency band which corresponds to the natural frequencies of the millimeter-sized bubbles in this study. The hydrophone is effectively omnidirectional in this band.

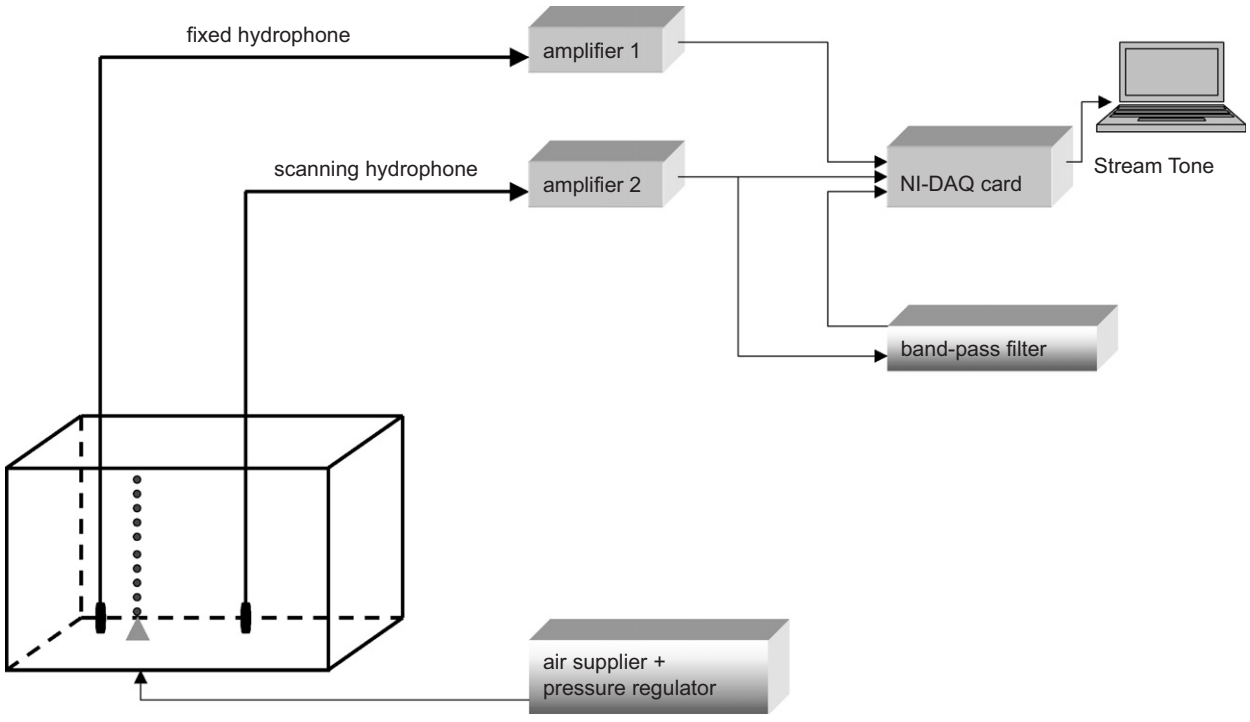

Fig. 1. Experimental set-up.

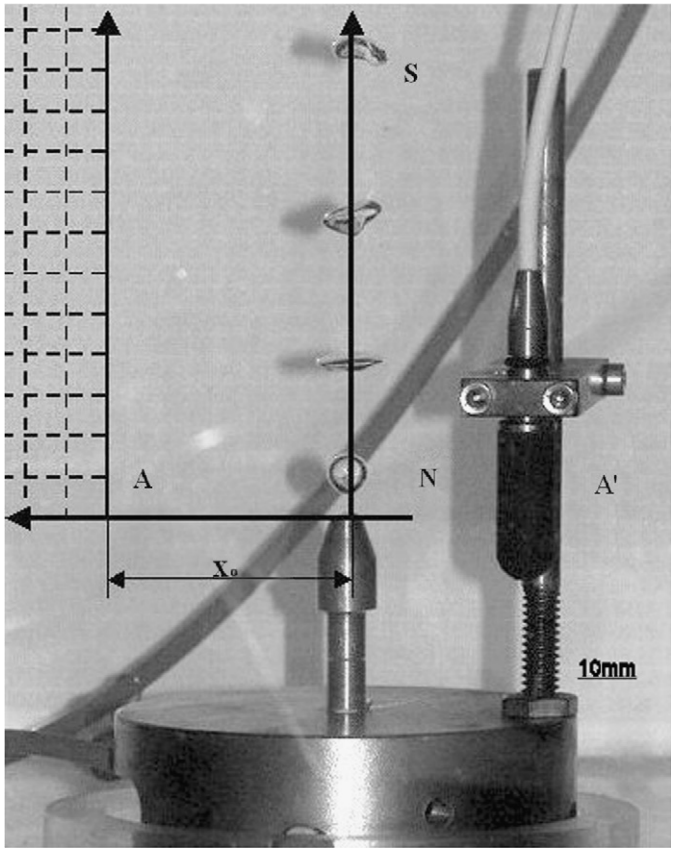

Fig. 2. Bubble chain.

The acoustic centre of the first (fixed) hydrophone was at a horizontal distance of $X_0 = 60$ mm (point A in Fig. 2) from the nozzle axis (N–S) and at the same level as the nozzle orifice. This position was maintained for all of the experiments while the Bubble Production Rate (BPR) was varied. The second (scanning) hydrophone was positioned on a 38×31 grid (20 mm point to point distance) within the vertical plane (N–S–A) containing the nozzle axis (N–S). The positioning of the second hydrophone was automatically controlled using a robot (S-Model 10, Type A05B-1024-B202, Fanuc Ltd.), permitting acquisition of a large amount of data over the grid.

2.2. Data acquisition

The hydrophone signals were pre-amplified by Bruel & Kjaer type 2635 charge amplifiers and digitized by a National Instruments Data Acquisition Card type 6024E. The signal from the scanning hydrophone (see Figs. 1 and 3) was amplified and filtered with a Stanford Digital SR560 band-pass filter. The pass band was 30 Hz–10 kHz which ensured that frequencies generated by the individual bubbles as well as most sub-harmonics due to collective bubble shape oscillations were preserved, while removing low-frequency fluctuations due to the rising motion of bubbles and unwanted high-frequency noise. The logging and recording of the voltage data is schematically shown in Fig. 3.

The acoustic pressure in the form of voltage output was stored in separate files using a program built on a LabView platform (National Instruments). The program consisted of one main program for controlling the robot and two sub-programs for data recording. The first sub-program was StreamTone (CSIRO), configured for two-channel recording. The first channel (CH0) was connected to the fixed hydrophone and the second channel (CH1) was connected to the filter and the scanning hydrophone (Fig. 3). The second sub-program was

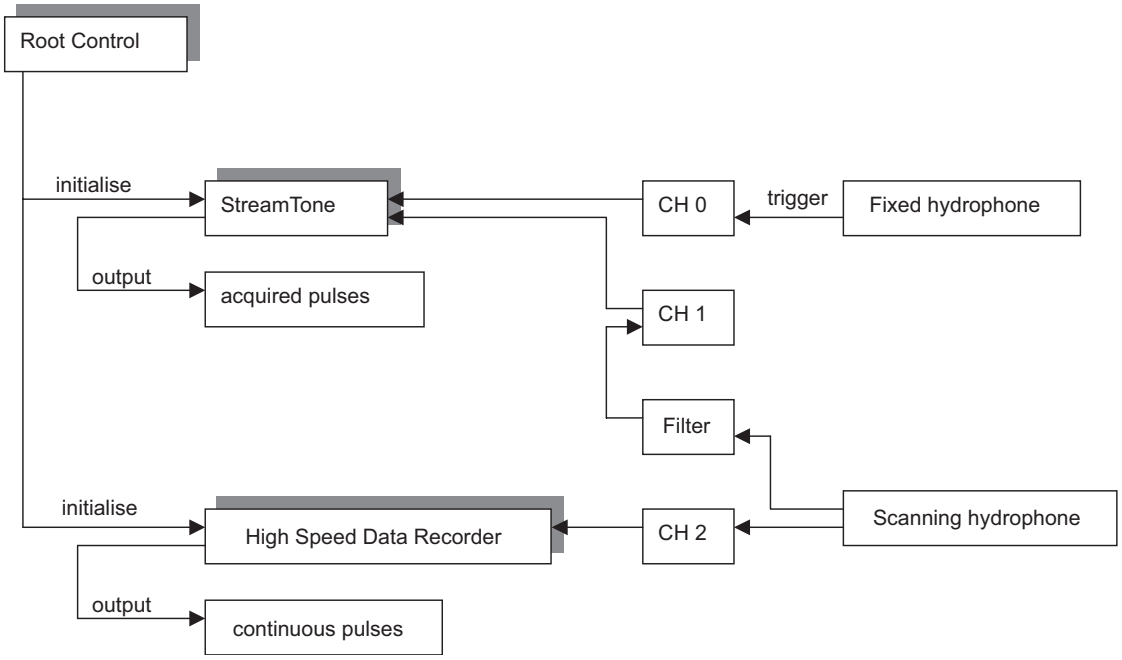

Fig. 3. Logging block diagram.

the High-Speed Data Recorder (National Instruments) for recording non-filtered and non-triggered (continuous) data from the third channel (CH2) which was connected to the scanning hydrophone.

A digital camera (Nikon Coolpix 5700) was used for capturing images and movies of bubbles formed at the nozzle. Digital movies of bubbly chains were recorded over a period of 1 min for each BPR. The images acquired for the bubble sizes were extracted as discrete frames from the movies. In addition, separate images with higher resolution were taken. An example of the images taken is shown in Fig. 2. Image processing was performed using ImageJ [35]. First the edge of the bubble was extracted from a sequence of photos, and the software calculated and displayed the edge area statistics. ImageJ approximates the bubble's edge with an ellipsoid. After calculating the volume of the ellipsoid, the equivalent radius of a sphere with the same volume is calculated. The bubble-sizing software was run on digitized bubble images and compared with data from the acoustic measurements. Since the bubbles at the point the image data is recorded are axisymmetric, this form of approximation has been shown to give an accuracy of 90% or better [40].

2.3. Recording procedure

Two channels, one for the fixed and one for the scanning hydrophone, were logged at 30 kHz each with a 12-bit resolution. The acoustic pressure from both hydrophones in the form of a digitized voltage was recorded at every grid point. The digitized waveforms contained 1024 data points (thus the data was recorded for a total of $T = 1024/30,000s = 34.13$ ms) for each bubble pulse. Between 36 and 40 pulses were recorded at each grid point. The recording of data was only initiated once a certain voltage trigger level was reached. The signal from the fixed hydrophone was used as the trigger because the signal near the nozzle is highly repeatable [36,37]. Once the triggering occurred, data was recorded on CHO and CH1 simultaneously (see Fig. 3). This provided coordinated acquisition of the sound signal from the source and the far field. Since, the hydrophones were different distances from the source there was a small delay time between the two signals owing to the finite speed of sound in water. The maximum possible delay was estimated to be approximately 0.5 ms. This is the shortest possible time for the disturbances in the system to be plotted in Section 3.3 below to travel the length of the chain, since as noted earlier, the presence of bubbles will reduce propagation speeds. The time delay was recently shown to be important in theoretical models of the phenomenon [33].

Once pulses of data had been recorded, a second program was initialized to record continuous data from channel CH2 for an unbroken 2–3 s, ensuring that approximately 30–60 bubble pulses were recorded (this was dependent on the BPR). After the data recording at a certain point was completed, the main program moved the robot arm to the next grid point and the recording procedure was repeated.

2.4. Voltage data mapping

The post-processing was conducted by using a MATLAB code that converts the voltage data into acoustic pressure. Visualization is possible because the instantaneous pressure field is calculated at each point in the grid. This information can be used to obtain information on the temporal and spatial variation of the pressure field. The hydrophone voltages (acoustic pressures) are represented by coloured contour levels in the images, and are linearly interpolated as appropriate for pixels that fall between any two adjacent grid points. These images, while relatively simple to create, can reveal a great amount of information about the acoustic field around the chain of bubbles.

2.5. Preliminary experiments—single bubble testing

Preliminary experiments were carried out to determine the size of the tank above which experimental measurements would be independent of the size of the tank. In these tests, the signal was measured from the formation of a single bubble. Experimental data were taken from tanks of different shapes and sizes. It was found that cylindrical tanks and small rectangular tanks significantly distort the signal due mainly to the reflections at the walls of the tank. Negligible distortion was found in rectangular tank with minimum dimension above 0.25 m. The data presented in this paper was obtained using a rectangular tank of size 0.95 m × 0.56 m × 1.5 m. As a final check, measurements were carried out in a roughly rectangular lake of size 100 m × 160 m and a depth of 16–18 m. Results were consistent with data from the rectangular laboratory tank reported here.

3. Results and analysis

3.1. Properties of the bubble chains

The experiments were designed to generate vertical bubble chains of different configurations. Table 1 shows details of the important parameters for the various bubble chains. Different BPRs (hence different bubble chain configurations) were obtained by varying the air pressure at the nozzle. Increasing the air pressure increases the potential energy in the system, and hence, the initial sound signal at bubble formation has a higher amplitude. For the bubbles produced by the 2.5 mm nozzle this amplitude starts with a value of 1.5 Pa for a BPR of 0.25 Hz up to 30 Pa for a BPR of 18 Hz. For the 1 mm nozzle, the values range from 1.0 Pa for a BPR of 0.25 Hz up to 20 Pa for a BPR of 38 Hz. The lowest investigated BPRs were limited by the signal-to-noise ratio. At very low BPRs this ratio drops dramatically, making the measurements of the bubble sound impossible at the farthest distance considered. At BPRs above 18 Hz, for the 2.5 mm nozzle, and at above 38 Hz, for the 1 mm nozzle, the bubbles start to collide and they cannot be identified as distinct discrete bubbles anymore. Photos of the bubble chain configurations at various BPR for the 1 mm nozzle is shown in Figs. 4 and 5.

As in all sparging systems, increasing the air pressure at the nozzle increases the bubble size as well as BPR. For the 2.5 mm nozzle, the average recorded bubble radius (from the photographs) was 2.5 mm for 0.25 Hz BPR and up to 3.7 mm for 18 Hz BPR. For the 1.0 mm nozzle, the average bubble radius was 1.0 mm for 0.25 Hz BPR and at 38 Hz BPR, the recorded bubble radius was 2.6 mm. The distance between the subsequent bubbles was decreased at higher BPR. For the 2.5 mm nozzle with a BPR of 10 Hz, the distance between the bubbles is 20 mm whereas when the BPR was increased to 18 Hz, the average distance between the bubbles was 14.1 mm. It is expected that there are stronger interactions of the acoustic field when the bubbles are closer together.

Table 1
Parameters of the experimentally generated and analysed bubble chain configurations

Nozzle	BPR (Hz)	Audio frequency (kHz)	Optical radius (mm)	Minnaert freq. (kHz)	Separation (mm)	Number of bubbles	$\beta \times 10^{-6}$ (m^3/s)
	0.25	2.97 ± 0.010	1.00 ± 0.010	2.97 ± 0.005	1200 ± 0.000	1 ± 0	0.0004
	8	1.97 ± 0.016	1.15 ± 0.011	2.15 ± 0.005	40.0 ± 0.010	32 ± 1	0.0905
	10	1.94 ± 0.010	1.18 ± 0.012	2.00 ± 0.005	36.0 ± 0.012	40 ± 1	0.1468
	12	1.90 ± 0.025	1.35 ± 0.013	1.93 ± 0.010	32.8 ± 0.014	48 ± 1	0.1888
	14	1.88 ± 0.015	1.41 ± 0.013	1.82 ± 0.010	30.0 ± 0.012	56 ± 2	0.2364
	18	1.80 ± 0.030	1.50 ± 0.014	1.72 ± 0.010	26.3 ± 0.013	72 ± 2	0.3267
1 mm	20	1.79 ± 0.045	1.52 ± 0.014	1.68 ± 0.010	19.7 ± 0.015	80 ± 2	0.3909
	22	1.68 ± 0.080	1.55 ± 0.014	1.64 ± 0.010	17.0 ± 0.016	88 ± 2	0.4300
	24	1.52 ± 0.075	1.64 ± 0.015	1.64 ± 0.010	16.0 ± 0.013	96 ± 3	0.5061
	26	1.21 ± 0.050	1.70 ± 0.016	1.60 ± 0.020	14.0 ± 0.014	104 ± 2	0.5927
	29	1.15 ± 0.020	1.88 ± 0.017	1.56 ± 0.020	10.3 ± 0.015	116 ± 3	0.7775
	31	1.06 ± 0.014	2.00 ± 0.018	1.53 ± 0.030	9.2 ± 0.017	124 ± 2	0.9865
	34	0.91 ± 0.010	2.10 ± 0.018	1.49 ± 0.030	7.5 ± 0.013	136 ± 2	1.2978
	38	0.84 ± 0.010	2.60 ± 0.019	1.31 ± 0.030	6.5 ± 0.012	152 ± 3	2.1652
	0.25	1.31 ± 0.010	2.50 ± 0.010	1.31 ± 0.010	1200 ± 0.000	1 ± 0	0.0052
	10	0.77 ± 0.010	2.70 ± 0.012	1.13 ± 0.010	20.0 ± 0.012	40 ± 1	1.0210
	12	0.76 ± 0.025	3.12 ± 0.013	1.06 ± 0.010	18.1 ± 0.014	48 ± 1	1.4970
2.5 mm	14	0.75 ± 0.015	3.31 ± 0.013	0.99 ± 0.010	17.2 ± 0.012	56 ± 2	2.1060
	16	0.73 ± 0.030	3.52 ± 0.014	0.93 ± 0.020	15.3 ± 0.013	64 ± 2	2.8720
	18	0.67 ± 0.030	3.70 ± 0.014	0.88 ± 0.020	14.1 ± 0.013	72 ± 2	3.8170

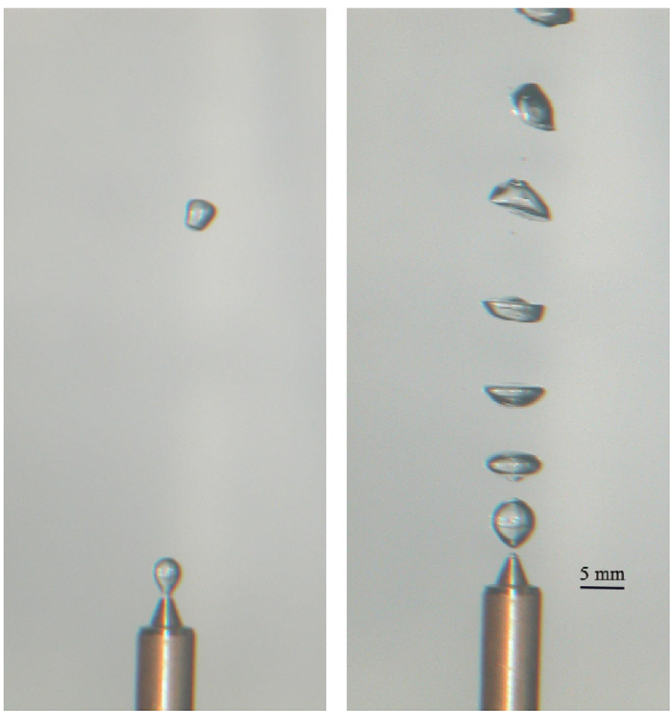

Fig. 4. Bubble chain at 10 Hz BPR (left) and 38 Hz BPR (right).

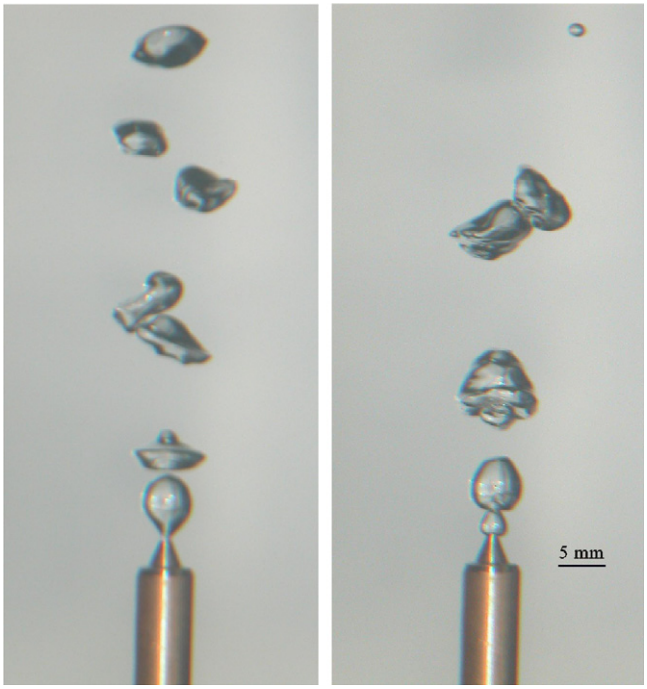

Fig. 5. Bubble chain at 40 Hz BPR (left) and 44 Hz BPR (right).

3.2. Measurements of bubble radius—acoustic versus optical

Two different methods were used to determine the size of the bubbles. The first was an acoustic method based on Minnaert's equation

$$f_0 = \frac{1}{2\pi R_0}\sqrt{\frac{3\gamma P_\infty}{\rho_l}}, \tag{1}$$

where R_0 is the equilibrium bubble radius, P_∞ is the hydrostatic pressure, γ is the adiabatic index and ρ_l is the density of the surrounding liquid. Eq. (1) shows a simple inverse relationship between the frequency of the bubble and its radius. This assumes that the bubble remains spherical and neglects damping, surface tension, liquid compressibility and vapour pressure, which do not have significant effects for the millimeter-sized bubbles considered here. The second method is by direct optical measurement from photographic images (as detailed in Section 2.5). This has been previously done by many authors [38–40]. The bubble-sizing software was run on the digitized bubble images and compared with the acoustic measurements. The results from these visual records were defined to determine the 'real' size and consequently the natural frequency of the bubbles.

Hence, two different frequencies (and corresponding bubble size based on Eq. (1)) can be calculated. Firstly, the spectrum of sound from the nearest point to the nozzle has a peak frequency which we will call f_{aud}. Secondly, the radius of the bubbles that was measured via the optical method R_{opt} has a corresponding natural frequency, f_{opt} calculated with Eq. (1). The difference between the results obtained through both methods are summarized in Table 1 and Fig. 6. The data show that acoustic bubble-sizing based simply on the peak of the pulse sound spectrum overestimates the size of the bubbles, consistent with earlier observations [17]. This discrepancy is even more marked at higher BPRs when more bubbles are introduced into the bubble chain. Manasseh et al. [17] showed how a time-domain rather than a spectral-peak method of measuring bubble size gave more accurate results, and the reason for the discrepancy was explained by Manasseh et al. [18]

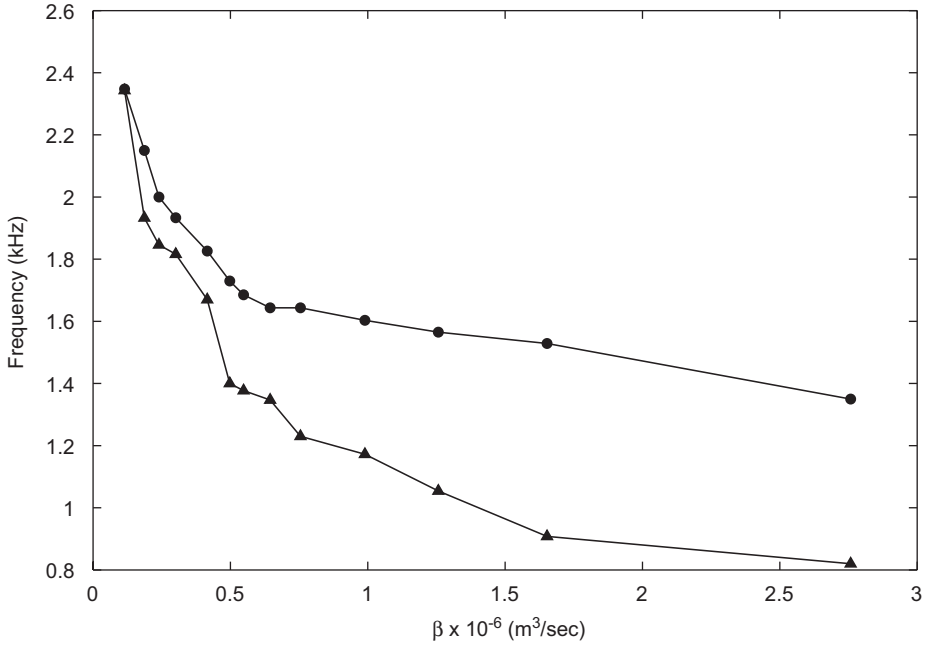

Fig. 6. Comparison of audio, $\triangle f_{\text{aud}}$, and optical, $\bullet f_{\text{opt}}$, measurements of the natural frequency of the bubble. β is the total volume of air in the bubble chain.

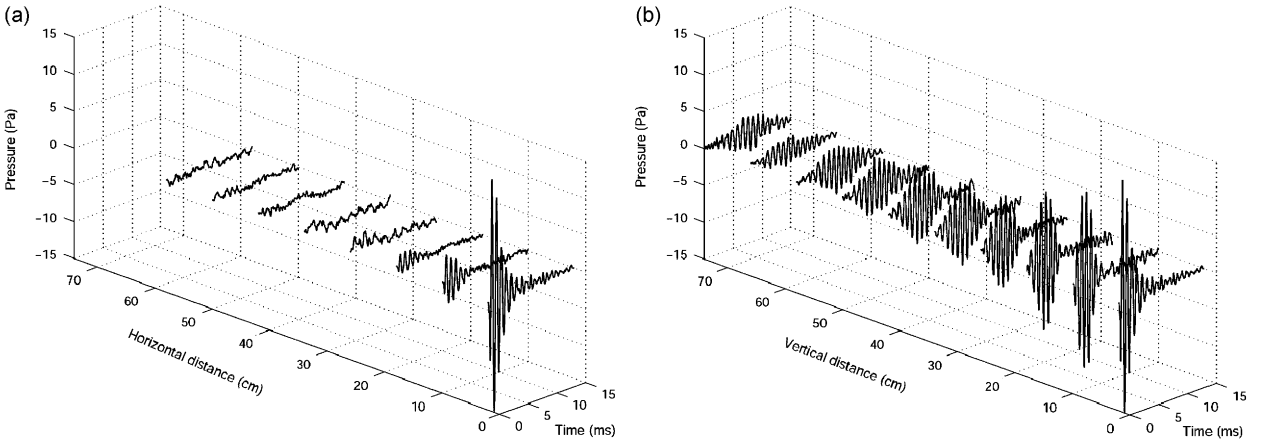

Fig. 7. Waveforms recorded by the scanning hydrophone in (a) the horizontal and (b) the vertical direction. Nozzle 1 mm, BPR 28 Hz.

3.3. Propagation of the acoustic energy

Typical waveforms recorded by the scanning hydrophone are shown in Fig. 7. The anisotropy between the vertical and horizontal directions noted previously [18,33] are apparent. The development and the propagation of the acoustic signal for a case when the bubble chain is generated by the 2.5 mm nozzle at 18 Hz BPR is demonstrated in a series of time frames (instantaneous pressure fields) in Fig. 8. The pressure scale is fixed from −5 Pa (deep blue) to +5 Pa (deep red); the green colour corresponds to 0 Pa (gauge pressure). The corresponding time is indicated at the top of each frame. The first row shows frames from the first part of the signal (0.23–1.233 ms). The effects of the other bubbles in the chain on the propagation of the acoustic signal can be seen. The acoustic pulse propagates in a form of a pressure wave creeping along the chain (indicated by

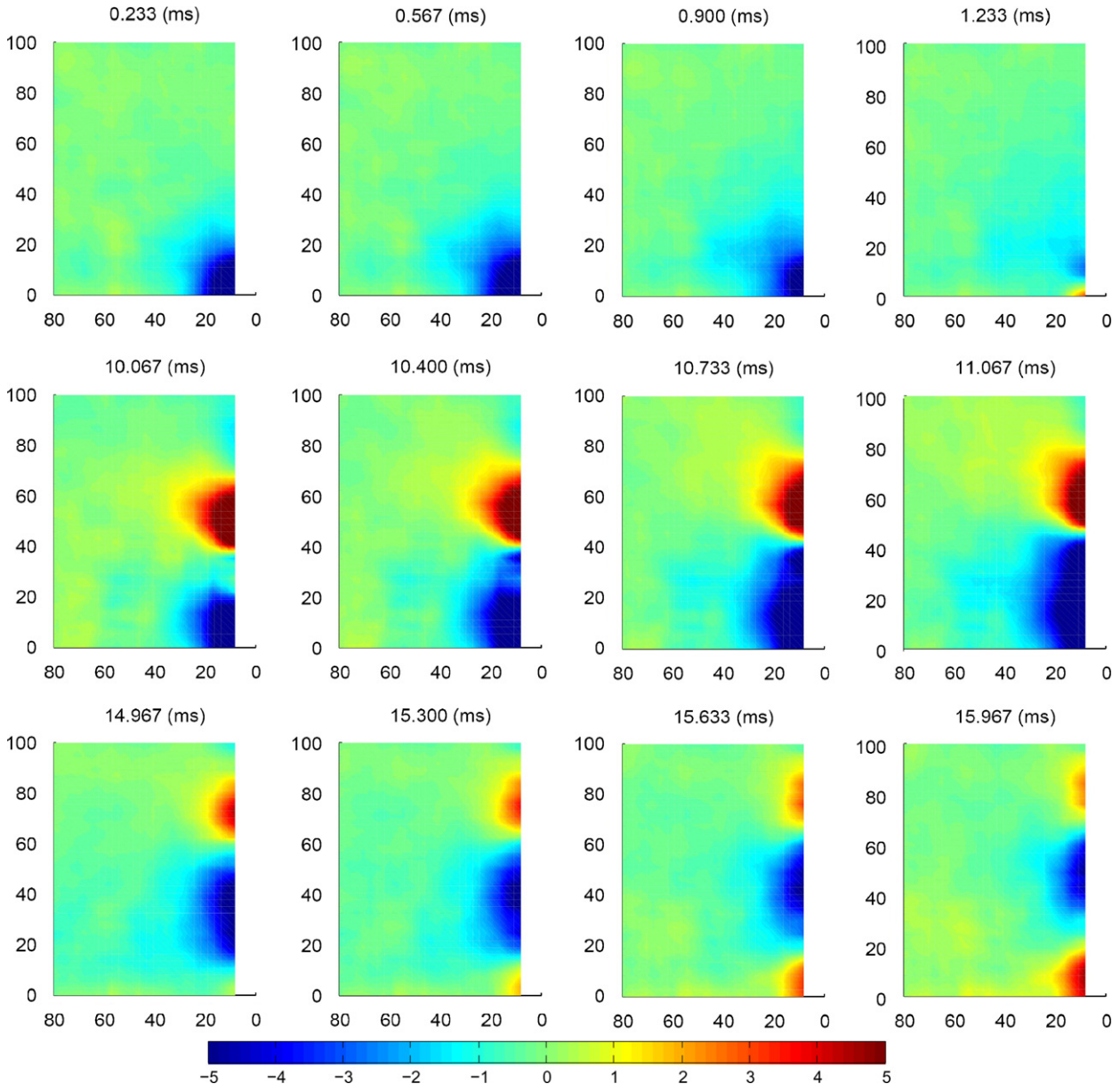

Fig. 8. Instantaneous pressure distribution of the pulse at the times noted above each frame. The bubble diameter is $D_0 = 7.4$ mm and the vertical and horizontal axes are r/D_0 and z/D_0, respectively. The colour originals of this figure can be seen on the journal's website; the first pressure extreme, which can be seen in the panel for 0.233 ms at top left, is negative; in the second and third rows, the uppermost pressure extreme is positive.

the blue surface). The second row illustrates the middle-time of the signal (i.e from 10.067 to 11.067 ms) and here there is more apparent anisotropy in the propagation of the acoustic signal. The positive (red) and negative (blue) pressures can be seen only along the chain. The third row shows four frames towards the end of the signal (from 14.967 to 15.967 ms). In this part of the acoustic pulse there are three different pressure sections occurring along the chain, each separated by roughly 40 bubble diameters (which corresponds to 0.296 m) and this is essentially the pressure wave that develops and propagates along the chain. It should be noted that at the frequency recorded by the fixed hydrophone is 0.67 kHz (see Table 1). Thus the wavelength of sound in pure water is about 2.2 m. Thus, the wavelength of the pressure variation along the chain is much shorter than the wavelength of sound in pure water.

Similar plots could be generated with the data from the 1 mm nozzle. This is shown in Fig. 9. Similarly to the case reported above, it is clear that there is a preference for acoustic energy to travel along the bubble chain. This phenomenon can be understood in qualitative terms as follows. Initially, only the newly formed bubble at the bottom is perturbed and the other bubbles are at equilibrium, since the pulses they produced on their formation have died off. The other bubbles are all the same size as the newly formed bubble and have almost identical resonant frequencies [18]. Hence, energy is rapidly absorbed from the newly formed bubble and re-distributed to the other 'parasite' bubbles. Subject to certain assumptions [18,32,33], the chain of bubbles can be regarded as a set of coupled oscillators. This can be imagined mechanically as, and is mathematically identical to, a series of masses on springs with each mass connected to neighbouring masses by springs. All such systems exhibit wavelike behaviour, with an oscillation initiated at one end of the system travelling to the other end, as observed here. As the number of bubbles becomes large and the spacing between them becomes small compared to the wavelength of the disturbance, the system's behaviour should be

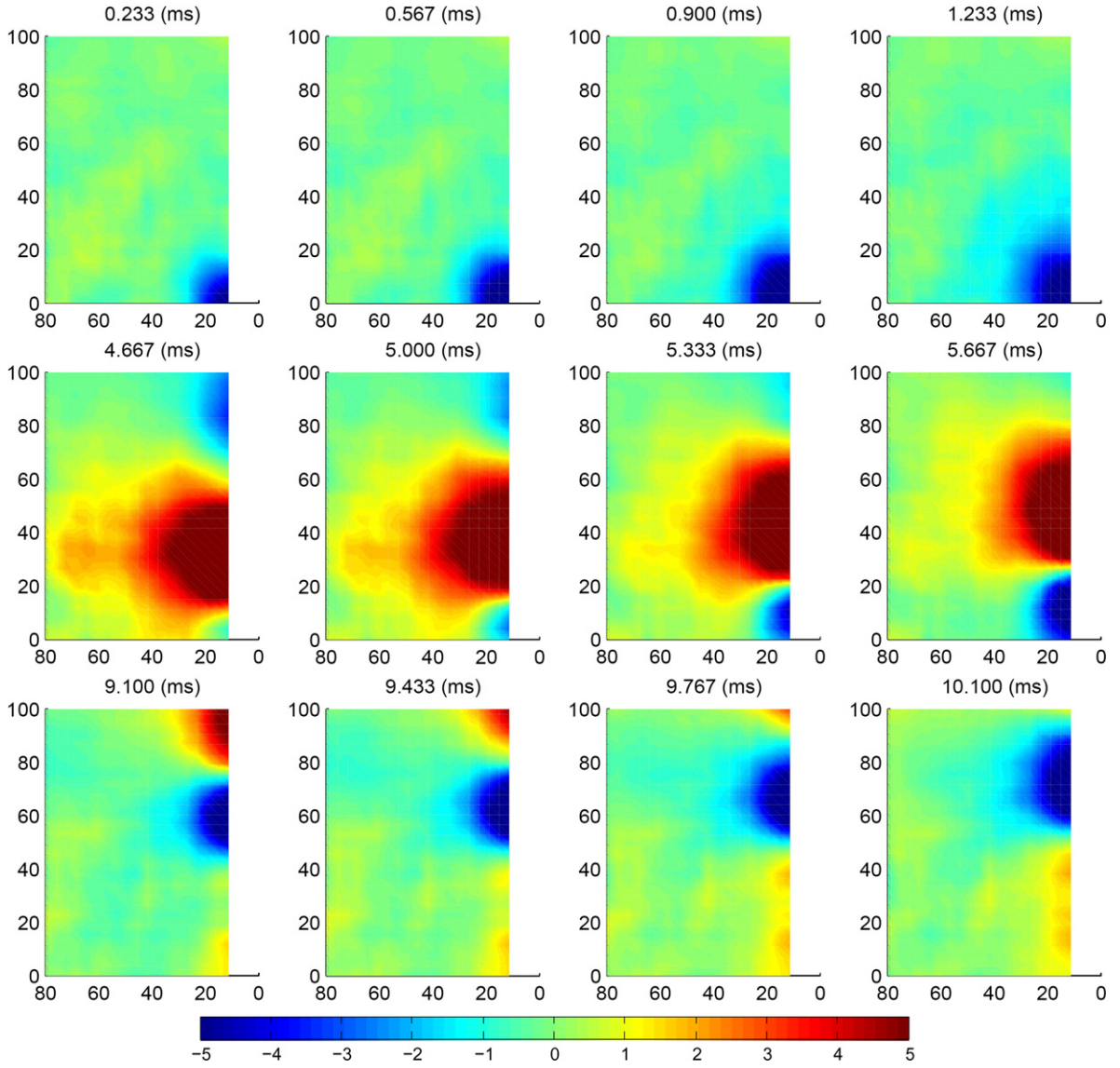

Fig. 9. Instantaneous pressure distribution of the pulse at the times noted above each frame. The bubble diameter is $D_0 = 5.2$ mm and the bubble production rate is 38 Hz. The vertical and horizontal axes are r/D_0 and z/D_0, respectively. The colour originals of this figure can be seen on the journal's website.

reducible to a continuum approximation in which waves propagate, albeit in a highly anisotropic fashion. It is worth noting that for the bubble chain, the 'connection' is provided by the pressure transmitted throughout the water. Thus, each mass is connected not only to its nearest neighbours by springs, but to all the other masses, by springs that are less stiff the more remote the connection.

Profiles of the pressure waves were taken at various times along a line parallel to the bubble chain (i.e. along line A–A″ in Fig. 2). It is interesting to note that the wavelength of this pressure profile is smaller at the bottom of the chain. At the top of the chain, the pressure profile has a longer wavelength. This is typical of all the profiles available in our data set. A MATLAB computer program was written to track the propagation of the peak pressure in order to calculate the speed of propagation of the acoustic energy along the chain. In practice, the experimental data can get quite noisy and needs to be filtered. Without filtering, it can take a long time (or is sometimes impossible) for the numerical algorithm to detect the local pressure maxima/minima. The fourth-order filter as described in Ref. [41] was used to perform filtering of the raw data. Typical effects of

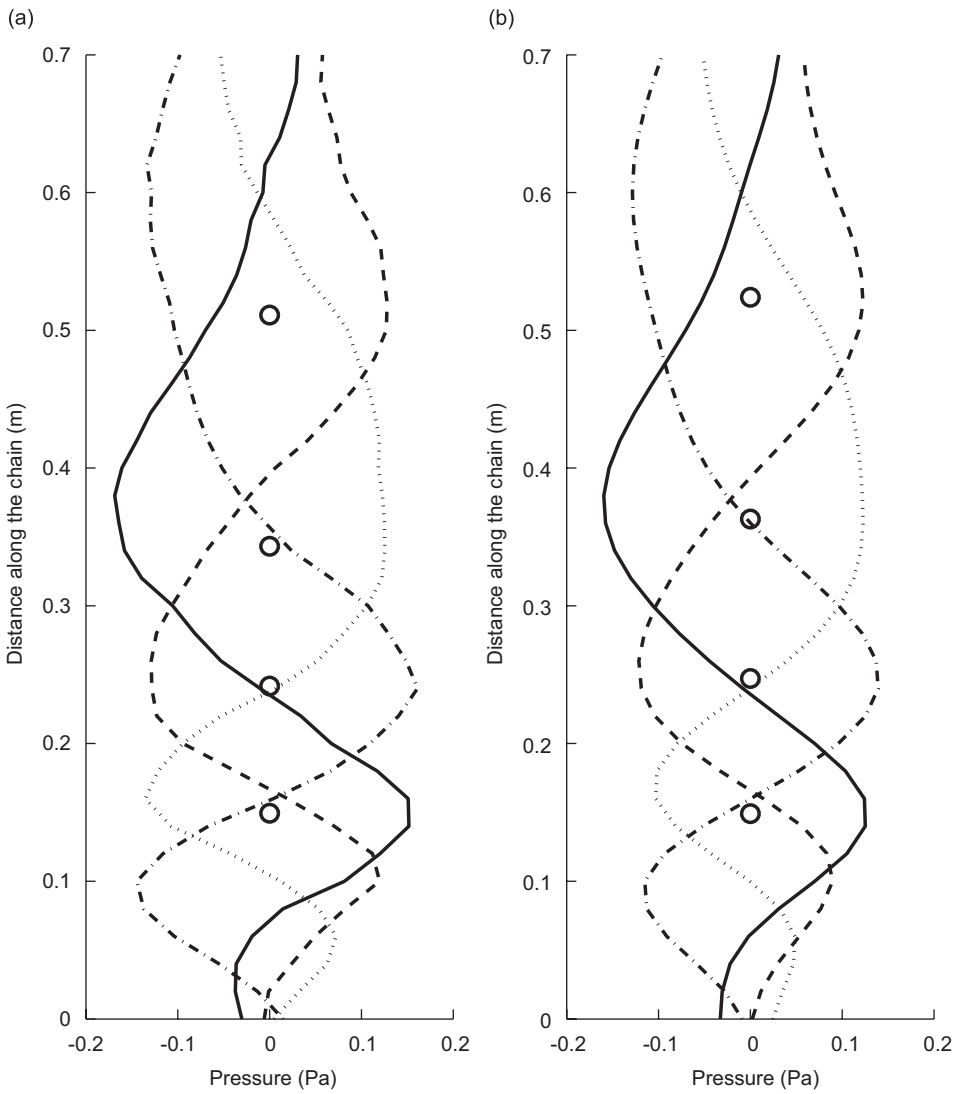

Fig. 10. Evolution of the pressure wave on a vertical line along the bubble chain. The vertical line is 6 cm from the bubble chain and the profiles shown are at times $t/T_0 = 7.2$ (—) 7.6 (– · –) 7.9 (· · · · ·) 8.3 (– – – –). The ○ in the figure indicates the position of the local maximum pressure detected by the computer program: (a) shows the raw experimental data and (b) shows the filtered data using the fourth-order filter as described in Ref. [41].

smoothing are shown in Fig. 10. The raw experimental data is shown in 10(a) and the filtered data is shown in 10(b). The figure was constructed with data from the 1 mm nozzle at 20 Hz BPR and the location of the pressure peak found by the MATLAB program is shown by the circle (○) in the figure. It is clear from this figure that the location of the pressure peak is only marginally affected by the filtering process. Filtering allows the local pressure maxima/minima to be located easily by the numerical algorithm.

The computer program was made to track the location of the peak pressure and subsequently calculate the instantaneous phase speed, V_p. When the pressure peak exits the domain, the computer program will find and track a new peak at the bottom of the bubble chain and compute its V_p. Fig. 11 shows the speed of propagation along the chain, V_p, as a function of the distance along the chain. The horizontal axis is normalized by the speed of sound in water (c). In general, it can be seen that the speed of propagation is smaller than the speed of sound in water, consistent with general expectations (see e.g. Ref. [34]). Fig. 11(a) shows data typical of the 1 mm nozzle. There is also a tendency for the speed of propagation to increase as the peak pressure moves up the bubble chain. The peak pressure typically travels slowly at the bottom of the chain. Near the top of the chain, it is travelling close to the speed of sound in water. Similar analysis computed using data from the 2.5 mm nozzle at BPR of 14 Hz is shown in Fig. 11(b). Note that in contrast to the data from the 1 mm nozzle, there is less variation in V_p as the acoustic pulse travels up the bubble chain. This observation is true for all data from the 2.5 mm nozzle. In general, a smaller nozzle suffers from the onset of chaotic bubbling at a lower airflow rate than a larger nozzle [42], resulting in more scattered data; this difference between nozzles in an bubble-acoustic experiment was noted by Manasseh et al. [17].

Fig. 12 shows the distribution of the normalized average phase velocity ($\langle V_p \rangle / c$) plotted as a function of the BPR. The averaging was calculated from $(5.0/f_0) < t < (T/4)$ where f_0 is the Minnaert frequency for the corresponding bubble size and $T = 34.1$ ms is total time period for the collection of data. In practice, this involves tracking and calculating the speed 7–8 pressure peaks from the bottom to the top of the bubble chain. For $t < 5.0/f_0$, no clear pressure peak could be found in the profile data because it is too early for any pressure signal to be detected. For $t > T/4$, most of the signal would have died away and hence, no clear pressure peak could be detected. For the 1 mm nozzle at a BPR of 8 Hz, $\langle V_p \rangle / c \approx 0.59$. As the airflow rate increases the values of the phase velocity decreases to a value of $\langle V_p \rangle / c \approx 0.33$ when the BPR is 38 Hz. Generally data for the 2.5 mm nozzle shows smaller values of V_p than the 1 mm nozzle. This is owing to the larger bubble size in the chain.

From these results it is clear that V_p is sensitive to the bubble chain configurations (i.e. the size and the spacing between subsequent bubbles). It is shown that the speed of propagation of acoustic energy is smaller

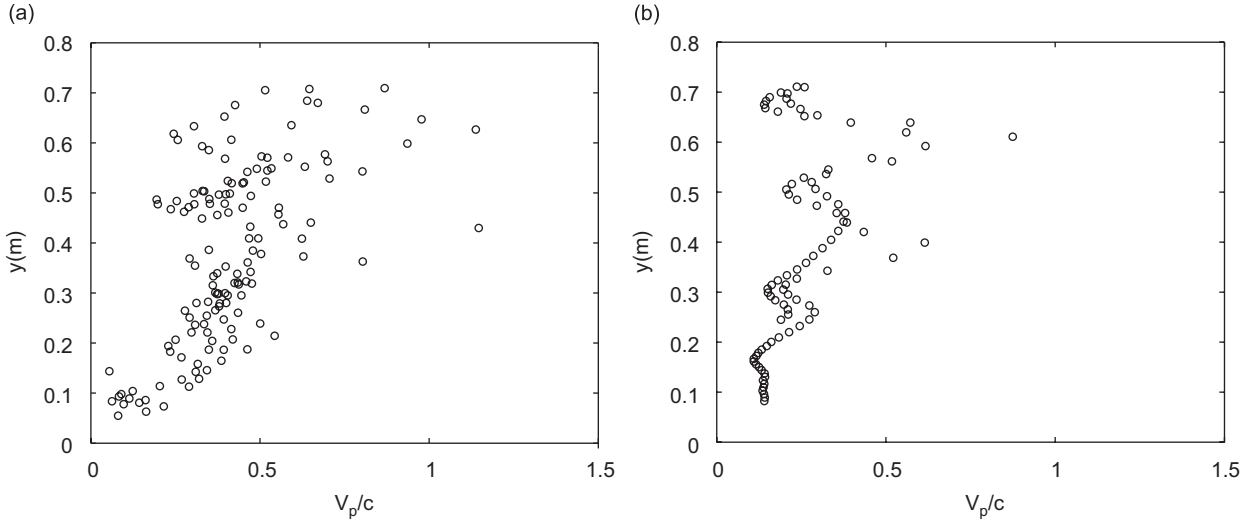

Fig. 11. Phase speed of acoustic energy along the chain: (a) data computed using data from the 1 mm nozzle with BPR of 20 Hz and (b) data computed using data from the 2.5 mm nozzle with BPR of 14 Hz.

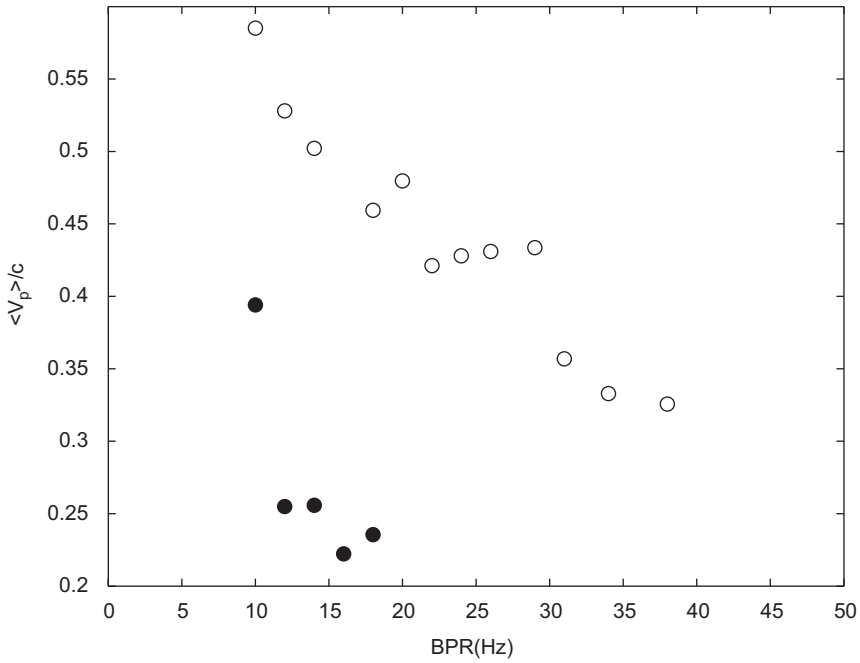

Fig. 12. Distribution of the average phase velocity parallel to bubble chains as a function of BPR. ○ data from 1 mm nozzle, • data from 2.5 mm nozzle.

than the speed of sound in water. The general trend in the experimental data is that as the airflow increases and when the chain consists of bigger bubbles, the speed of propagation of acoustic energy tend to decrease.

3.4. Averaged distribution of the pressure field

This 'localization' of the sound field along the chain is enhanced at higher BPRs. Fig. 13 shows the difference in the distribution of the P_{rms} for one bubble (left) and along the bubble chain (generated by the 1 mm nozzle at 30 Hz BPR). The grey scale corresponds to the pressure scale in Pascals and the dimensions represent the distance from the nozzle axis in horizontal and vertical direction. For evaluation six iso-lines are also indicated (0.3, 1, 2, 3, 4, 5 Pa). This anisotropic sound distribution around a bubble chain is consistent with the observation by Manasseh et al. [18], who noticed the phenomenon in measurements along a single horizontal and vertical line in a smaller tank.

3.5. Main attenuation trends

In this subsection the attenuation of the acoustic energy is analysed. The attenuation is calculated for the predominant (or peak) frequency in the signal recorded at the point closest to the point of bubble's formation, i.e. the attenuation is defined as

$$\frac{20}{L}\log\left(\frac{p_i}{p_0}\right), \tag{2}$$

where p_i is the peak value of the maximum in the FFT of the signal recorded at point i. This is the signal recorded with the scanning hydrophone. p_0 is the peak value of the maximum in the FFT of the signal recorded at point 0, this is the signal recorded with the fixed hydrophone. L is the distance between point i and point 0.

The experimentally measured profiles of the attenuation of the predominant frequency along the closest vertical line parallel to the bubble chains is plotted with black lines in Fig. 14, for a case when the 1 mm nozzle

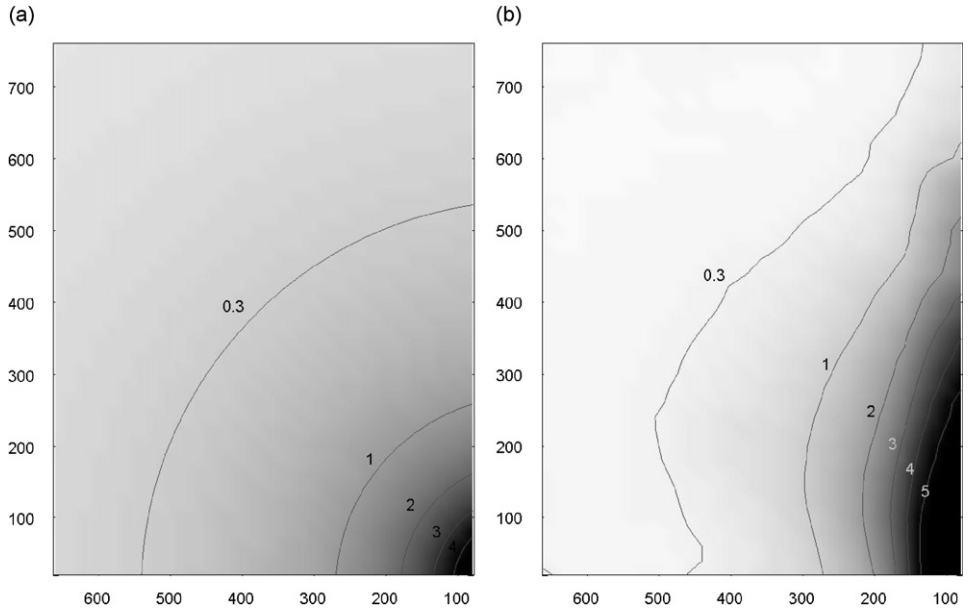

Fig. 13. Field distribution of P_{rms} in Pa for one bubble (left) produced by the 1 mm nozzle and for a bubble chain generated by the 1 mm nozzle at 30 Hz (right). Note that for comparison of the spatial distributions, pressure in the single-bubble field (left) has been multiplied by 15.

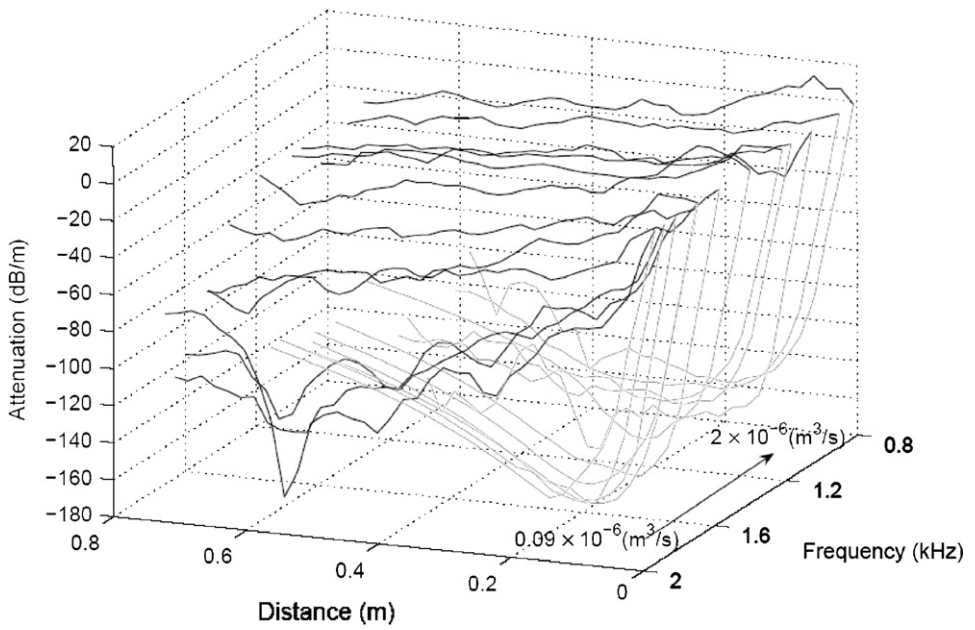

Fig. 14. Distribution of the attenuation in the vicinity of bubble chains formed by a 1 mm nozzle. The black lines are the attenuation measured along the bubble chains (i.e. along direction A–A″ in Fig. 3) and the grey lines are the attenuation away from the bubble chains (i.e. in direction N–A in Fig. 3).

was used (the same trend occurs along the bubble chain configurations generated with the 2.5 mm nozzle). The same profiles but along a line perpendicular to the axis of the bubble chains are indicated with grey lines. The profiles are plotted in three dimensions as a function of the frequency for which the attenuation is calculated and the distance from the tip of the nozzle. The arrow indicates the direction of the increased airflow rate.

As shown in Fig. 14, the difference between the attenuation of the measured sound pulse along and away from the chain axis is significantly increased with the increase of the airflow rate. At a low airflow rate of around $0.9 \times 10^{-6}\,m^3/s$ (a BPR of 10 Hz) the difference in the attenuation of the peak frequency along and away from the bubble chain is in the range of $-60 \pm 10\,dB/m$. As the airflow rate increases and the bubble chains become more closely-spaced, the difference in the attenuation becomes more significant, reaching a value of $-160 \pm 10\,dB/m$ at the highest investigated airflow rate of $2.8 \times 10^{-6}\,m^3/s$ (which had a BPR of 38 Hz).

For both nozzles it can be concluded that the attenuation of the signal's peak frequency is significantly reduced in the vicinity of the bubble chains, and that this effect is more significant as the number of bubbles in the chain is increased.

4. Conclusions

The acoustic field around vertical chains of rising bubbles has been mapped in high resolution in a vertical plane as a function of time. A special robotic traversing system was developed to obtain these data. The bubbles are continually produced by a system that ensures the size of the bubbles is constant. The acoustic excitation of the bubble chain is the sound naturally emitted by each bubble as it detaches from a nozzle. The results confirm earlier, low-resolution and time-averaged findings of a highly anisotropic sound pressure distribution around the chain [18,33]. The new time-dependent data clearly show a 'creeping wave' propagating along the bubble chain. Acoustic energy is basically redirected and channelled along the bubble chain, owing to the chain acting as a series of coupled oscillators [18,33]. Attenuation of the signal was found to be up to 160 dB/m greater in the horizontal than along the chain. This suggests that underwater noise from a bubble source could be transmitted towards the surface much more efficiently than horizontally.

The present results also allow the speed of propagation of the signal along the chain to be quantified. The speed of propagation of acoustic energy along the bubble chain dropped to values as low as about $0.2c$, where c is the speed of sound in pure water, for the case where the spacing between the bubbles are closest. It is widely known that sound speeds in homogeneous and isotropic bubbly flows can be greatly reduced [34] but here a speed reduction has been observed in a system that is clearly inhomogeneous and anisotropic. The present data also show the speed varies along the chain, suggesting that sound waves along the bubble chain are dispersive. It is worth noting that the measurements of this creeping wave were not made along the axis of the bubble chain but along a parallel line 6 cm from the nozzle. Presumably even more significant speed reductions occur closer to the axis of the bubble chain.

Acknowledgements

This work is supported and funded by the University of Melbourne through MIRS and MIFRS grants (Ref: 00-1456) and by Defence Science and Technology Organization (DSTO) and the Commonwealth Scientific and Industrial Research Organisation (CSIRO) through the SPR Studentship. Tony Kilpatrick and Lachlan Graham at the CSIRO wrote the experimental control and data acquisition routines and we are also grateful to Danny Stephenson for the construction of the apparatus.

References

[1] Z. Ye, Recent development in underwater acoustics: acoustic scattering from single and multiple bodies, *Proceedings of the National Science Council* 25 (2001) 137–149.

[2] N. Gorska, D. Chu, Some aspects of sound extinction by zooplankton, *Journal of the Acoustical Society of America* 110 (2001) 2315–2325.

[3] T.K. Stanton, P.H. Wiebe, D. Chu, Differences between sound scattering by weakly scattering spheres and finite-length cylinders with applications to sound scattering by zooplankton, *Journal of the Acoustical Society of America* 103 (1998) 254–264.

[4] K.W. Commander, A. Prosperetti, Linear pressure waves in bubbly liquids: comparison between theory and experiments, *Journal of the Acoustical Society of America* 85 (1989) 732–746.

[5] N.Q. Lu, A. Prosperetti, S.W. Yoon, Underwater noise emission from bubble clouds, *Journal of Oceanic Engineering* 15 (1990) 275–281.

[6] Z. Ye, C. Feuillade, Sound scattering by an air bubble near a plane sea surface, *Journal of the Acoustical Society of America* 102 (1997) 798–805.
[7] I. Tolstoy, Properties of superresonant systems of spherical scatterers, *Journal of Oceanic Engineering* 12 (1987) 327–332.
[8] P.H. Calderbank, Physical rate processes in industrial fermentation, part i: the interfacial area in gas–liquid contacting with mechanical agitation, *Transactions of the Institute of Chemical Engineering* 36 (1958) 443–463.
[9] F. Takemura, A. Yabe, Gas dissolution process of spherical rising gas bubbles, *Chemical Engineering Science* 53 (15) (1998) 2691–2699.
[10] J.W.R. Boyd, J. Varley, The uses of passive measurement of acoustic emissions from chemical engineering processes, *Chemical Engineering Science* 56 (2001) 1749–1767.
[11] R. Manasseh, C. Forbes, K. Rickards, I. Bobevski, A. Ooi, Passive acoustic determination of wave-breaking events and their severity across the spectrum, *Journal of Atmospheric and Oceanic Technology* 23 (4) (2006) 599–618.
[12] K.W. Commander, A. Prosperetti, Linear pressure waves in bubbly liquids: comparison between theory and experiments, *Journal of the Acoustical Society of America* 85 (2) (1989) 732–746.
[13] A.D. Phelps, D.G. Ramble, T.G. Leighton, The use of a combination frequency technique to measure the surf zone bubble population, *Journal of the Acoustical Society of America* 101 (4) (1996) 1981–1989.
[14] R. Duraiswami, S. Prabhukumar, G.L. Chahine, Bubble counting using an inverse scattering method, *Journal of the Acoustical Society of America* 104 (5) (1998) 2699–2717.
[15] G.L. Chahine, K.M. Kalumuck, J.-Y. Cheng, G.S. Frederick, Validation of bubble distribution measurements of the ABS acoustic bubble spectrometer with high speed video photography, *Fourth International Symposium on Cavitation*, San Diego, USA, June 2001, Paper A7-004, 2001.
[16] E.J. Terrill, K.W. Melville, A broadband acoustic technique for measuring bubble size distributions: laboratory and shallow water measurements, *Journal of Atmospheric and Oceanic Technology* 17 (2000) 220–239.
[17] R. Manasseh, R.F. LaFontaine, J. Davy, I. Shepherd, Y. Zhu, Passive acoustic bubble sizing in sparged systems, *Experiments in Fluids* 3 (23) (2003).
[18] R. Manasseh, A. Nikolovska, A. Ooi, A. Yoshida, Anisotropy in the sound field generated by a bubble chain, *Journal of Sound and Vibration* 278 (4–5) (2004) 807–823.
[19] M. Ruzicka, Vertical stability of bubble chain: multiscale approach, *International Journal of Multiphase Flow* 31 (2005) 1063–1096.
[20] E.A. Zabolotskaya, Interaction of gas bubbles in a sound field, *Soviet Physics Acoustics* 30 (5) (1984) 365–368.
[21] H. Ogũz, A. Prosperetti, A generalization of the impulse and virial theorems with an application to bubble oscillations, *Journal of Fluid Mechanics* 218 (1990) 143–162.
[22] A.A. Doinikov, S.T. Zavtrak, On the mutual interaction of two gas bubbles in a sound field, *Physics of Fluids* 7 (8) (1995) 1923–1930.
[23] I. Tolstoy, Superresonant systems of scatterers, i, *Journal of the Acoustical Society of America* 80 (1986) 282–294.
[24] I. Tolstoy, A. Tolstoy, Superresonant systems of scatterers, ii, *Journal of the Acoustical Society of America* 83 (1988) 2086–2096.
[25] C. Feuillade, Scattering from collective modes of air bubbles in water and the physical mechanism of superresonances, *Journal of the Acoustical Society of America* 98 (1995) 1178–1190.
[26] M. Ida, A characteristic frequency of two mutually interacting gas bubbles in an acoustic field, *Physics Letters A* 297 (3–4) (2002) 210–217.
[27] V. Twersky, Multiple scattering of waves and optical phenomena, *Journal of Optical Society of America* 52 (1962) 145–171.
[28] J.L. Leander, A note on transient underwater bubble sound, *Journal of the Acoustical Society of America* 103 (1998) 1205–1208.
[29] D.E. Weston, Acoustic interaction effects in arrays of small spheres, *Journal of the Acoustical Society of America* 39 (1966) 316–322.
[30] C. Feuillade, M.F. Werby, Resonances of deformed gas bubbles in liquids, *Journal of the Acoustical Society of America* 96 (1994) 3684–3692.
[31] P.Y. Hsiao, M. Devaud, J. Bacri, Acoustic coupling between two air bubbles in water, *European Physics Journal E* 4 (2001) 5–10.
[32] E. Payne, S. Illesinghe, A. Ooi, F. Manasseh, Symmetric mode resonance of bubbles attached to a rigid boundary, *Journal of the Acoustical Society of America* 118 (5) (2005) 2841–2849.
[33] A.A. Doinikov, R. Manasseh, A. Ooi, On time delays in coupled multibubble systems, *Journal of the Acoustical Society of America* 117 (1) (2005) 47–50.
[34] A. Wood, *A Textbook of Sound*, Bell & Sons, London, 1932.
[35] T. Collins, *ImageJ Image Processing and Analysis in Java*, first ed., Wright Cell Imaging Facility, Toronto Western Research Institute, MC 13 407, 399 Bathurst Street, Toronto, May 2004.
[36] A. Nikolovska, R. Manasseh, A. Ooi, Visualizing the acoustic field around bubbles using a hydrophone—scanning method, *The Seventh Asian Symposium on Visualization*, Singapore, 2003.
[37] R. Manasseh, S. Yoshida, M. Rudman, Bubble formation processes and bubble acoustic signals, *Third International Conference on Multiphase Flow*, Lyon, France, 1998.
[38] A.L. Tassin, D.E. Nikitopoulos, Non-intrusive measurements of bubble size and velocity, *Experimental Fluids* 19 (1995) 121–132.
[39] K. Lunde, R. Perkins, A method for the detailed study of bubble motion and deformation, in: A. Serizawa, T. Fukano, J. Bataille (Eds.), *Proceedings of the Second International Conference on Multiphase Flow*, Elsevier Science B.V., Amsterdam, 1996, pp. 395–405.
[40] A. Vazquez, R.M. Sanchez, E. Salinas-Rodríguez, A. Soria, R. Manasseh, A glance at three measurement techniques for bubble size determination, *Experimental Thermal and Fluid Science* 30 (1) (2005) 49–57.
[41] C.A. Kennedy, M.H. Carpenter, Several new numerical methods for compressible shear-layer simulations, *Applied Numerical Mathematics* 14 (1994) 397–433.
[42] R. Clift, J.R. Grace, M.E. Weber, *Bubbles, Drops and Particles*, Academic Press, London, 1978.